Identification of two segments of the γ subunit of ATP synthase responsible for the different affinities of the catalytic nucleotide-binding sites

Received for publication, February 17, 2018, and in revised form, November 26, 2018 Published, Papers in Press, December 3, 2018, DOI 10.1074/jbc.RA118.002504

Nelli Mnatsakanyan[1,2], **Yunxiang Li**[1,3], **and Joachim Weber**[4]

From the Department of Chemistry and Biochemistry, Texas Tech University, Lubbock, Texas 79409 and the Center for Membrane Protein Research, Texas Tech University Health Sciences Center, Lubbock, Texas 79430

Edited by Norma M. Allewell

ATP synthase uses a rotary mechanism to couple transmembrane proton translocation to ATP synthesis and hydrolysis, which occur at the catalytic sites in the β subunits. In the presence of Mg^{2+}, the three catalytic sites of ATP synthase have vastly different affinities for nucleotides, and the position of the central γ subunit determines which site has high, medium, or low affinity. Affinity differences and their changes as rotation progresses underpin the ATP synthase catalytic mechanism. Here, we used a series of variants with up to 45- and 60-residue-long truncations of the N- and C-terminal helices of the γ subunit, respectively, to identify the segment(s) responsible for the affinity differences of the catalytic sites. We found that each helix carries an affinity-determining segment of ~10 residues. Our findings suggest that the affinity regulation by these segments is transmitted to the catalytic sites by the DELSEED loop in the C-terminal domain of the β subunits. For the N-terminal truncation variants, presence of the affinity-determining segment and therefore emergence of a high-affinity binding site resulted in WT-like catalytic activity. At the C terminus, additional residues outside of the affinity-determining segment were required for optimal enzymatic activity. Alanine substitutions revealed that the affinity changes of the catalytic sites required no specific interactions between amino acid side chains in the γ and $\alpha_3\beta_3$ subunits but were caused by the presence of the helices themselves. Our findings help unravel the molecular basis for the affinity changes of the catalytic sites during ATP synthase rotation.

F_1F_o-ATP synthase catalyzes the final step of oxidative phosphorylation and photophosphorylation, the synthesis of ATP from ADP and P_i. F_1F_o-ATP synthase consists of the membrane-embedded F_o subcomplex with, in most bacteria, a subunit composition of ab_2c_{10} and the peripheral F_1 subcomplex with a subunit composition of $\alpha_3\beta_3\gamma\delta\epsilon$. The energy necessary for ATP synthesis is derived from an electrochemical transmembrane proton (or, in some organisms, sodium ion) gradient. Proton flow, down the gradient, through F_o is coupled to ATP synthesis on F_1 by a unique rotary mechanism. The protons flow through (half) channels at the interface of a and c subunits, which drives rotation of the ring of c subunits. The c_{10} ring, together with F_1 subunits γ and ε, forms the rotor. Rotation of γ leads to conformational changes in the catalytic nucleotide-binding sites on the β subunits where ADP and P_i are bound. The conformational changes result in formation and release of ATP. Thus, ATP synthase converts electrochemical energy, the proton gradient, into mechanical energy in the form of subunit rotation and back into chemical energy as ATP. In bacteria, under certain physiological conditions, the process runs in reverse. ATP is hydrolyzed to generate a transmembrane proton gradient, which the bacterium requires for such functions as nutrient import and locomotion (1–6).

F_1 (or "F_1-ATPase") has three catalytic nucleotide-binding sites, located on the three β subunits, at the interface to the adjacent α subunit. The catalytic sites have pronounced differences in their affinity for Mg^{2+}-nucleotide. In *Escherichia coli*, K_{d1} for MgATP is in the nanomolar range ("high-affinity site"), K_{d2} is ≈1 μM ("medium-affinity site"), and K_{d3} is ≈30–100 μM ("low-affinity site") (7, 8). The affinity of a catalytic site at any given point of time is determined by the position of the central γ subunit. This implies that during rotational catalysis the affinities change. After rotation of γ by 120°, the sites have swapped their affinities. Experimental evidence for the crucial role of γ in determining the affinities of the catalytic sites comes from observations of the dependence of substrate binding and product release on the rotational angle of γ (9–13). Further support is provided by the discovery of mutations in β at the β/γ interface that affect nucleotide binding affinities despite the fact that these mutations are located in the DELSEED loop in the C-terminal domain (14, 15), ≥30 Å away from the catalytic binding site.

The affinity differences and changes seem to be of central importance for the enzymatic mechanism with respect to coupling between rotation and catalysis as well as catalysis itself. ATP synthesis and hydrolysis occur only on the high-affinity

Part of this work was supported by National Institutes of Health Grant GM071462 (including American Recovery and Reinvestment Act Administrative Supplement) (to J. W.). The authors declare that they have no conflicts of interest with the contents of this article. The content is solely the responsibility of the authors and does not necessarily represent the official views of the National Institutes of Health.

This article contains Figs. S1–S3 and Tables S1 and S2.

[1] Both authors contributed equally to this work.
[2] Present address: Dept. of Internal Medicine, Yale University School of Medicine, New Haven, CT 06520.
[3] Present address: Dept. of Chemistry and Biochemistry, Texas Woman's University, Denton, TX 76204.
[4] To whom correspondence should be addressed: Dept. of Chemistry and Biochemistry, Texas Tech University, Box 41061, Lubbock, TX 79409-1061. Tel.: 806-834-6379; Fax: 806-742-1289; E-mail: joachim.weber@ttu.edu.

site (16). According to most catalytic models, in ATP synthesis proton translocation–driven rotation of γ forces the high-affinity site open, thereby reducing the affinity to "low" so that the newly formed ATP can be released (2, 17–19). In ATP hydrolysis, closing of the low-affinity site around the newly bound ATP, accompanied by conversion of the site to high-affinity, is widely believed to push γ and make it rotate for the experimentally observed 80° substep. The subsequent 40° substep appears to be energetically linked to the release of P_i and/or ADP (2, 12, 15, 17, 20–22).

Although a coherent picture of the general chemomechanical coupling mechanism is emerging, many aspects of the mechanism on the molecular level are still unresolved. For one, knowledge of the interactions between γ and β (and/or α) that are responsible for the different affinities of the catalytic binding sites is fragmentary. The majority of contacts between γ and the $\alpha_3\beta_3$ ring involve the long N- and C-terminal helices of γ.

Because of the large number of interactions that might possibly contribute, the first goal of the present study was to identify regions of γ that play a role in the assignment of affinities. In search of a screening method that allows looking at multiple residues at the same time, our approach was based on the observation that it is possible to generate mutants in ATP synthase from *Geobacillus stearothermophilus* (formerly known as *Bacillus* PS3) that have portions of the N- and/or C-terminal helices removed (23–26). We measured binding of MgATP to a series of N- and C-terminal truncation mutants in the *G. stearothermophilus* $\alpha_3\beta_3\gamma$ subcomplex. For both helices, increasing the length of the truncation converted the MgATP binding behavior from asymmetric and WT-like, with a clearly present high-affinity site, to (nearly) symmetric, as also observed in the complete absence of γ. This approach allowed us to narrow down the region of γ causing the differences in affinity of the catalytic sites to two short segments of ~10 residues, one in each helix.

To possibly identify individual residues responsible for conferring the nucleotide binding asymmetry, we replaced the amino acids in these two segments in groups of 5–6 residues by alanine. MgATP binding experiments with the alanine-replacement mutants all gave the WT-like asymmetric binding pattern. These results suggest that there is no specific residue in γ that causes the pronounced affinity differences of the three catalytic nucleotide-binding sites. Instead, the α-helices of γ themselves in the identified region appear to be the cause.

Results

Selection of enzyme source

The enzymes from *E. coli* and *G. stearothermophilus* (formerly *Bacillus* PS3) are arguably the best-characterized bacterial ATP synthases. They are sufficiently closely related so that the *G. stearothermophilus* F_1 subcomplex can be reconstituted with *E. coli* F_o to give a functional ATP synthase and vice versa (27). For the present study, we chose the *G. stearothermophilus* enzyme because of its higher oligomeric stability. Specifically, it could be shown that the *G. stearothermophilus* ATP synthase can form an $\alpha_3\beta_3$ complex in the absence of γ (28) that is stable enough to be crystallized (29) or monitored in high-speed atomic force microscopy (30). Under appropriate storage conditions, as ammonium sulfate precipitate at 4 °C, even after several years about two-thirds of the complex was still in $\alpha_3\beta_3$ form with about 20% isolated α and β subunits and the remainder unidentified degradation products, which are absent directly after preparation of the enzyme (Fig. S1). Thus, truncations of γ should not affect the stability of the $\alpha_3\beta_3$ complex.

N-truncation mutants of γ: an overview

The following N-terminal truncation mutants of the γ subunit of *G. stearothermophilus* ATP synthase $\alpha_3(\beta Y341W)_3\gamma$ subcomplex were generated: γΔN4, missing the first 4 residues of γ; γΔN9; γΔN13; γΔN29; and γΔN45 (the numbering system assumes that *E. coli*, used to express the *G. stearothermophilus* enzyme, removes the Met encoded by the start codon as is observed for the native *E. coli* ATP synthase). Subcomplexes with full-length γ, and γ-less subcomplex were included as controls. The γΔN45 mutant eliminates all contacts between the N-terminal helix of γ and the $\alpha_3\beta_3$ cylinder (31–33). The crystal structures of mitochondrial (31, 32) and *E. coli* F_1 (33) indicate that the N-terminal helix of γ starts immediately at the N terminus. Secondary structure predictions suggest that the same applies to *G. stearothermophilus* WT γ and to the truncation mutants investigated here (Fig. 1*A*) with the possible exception of the γΔN9 mutant. For the γΔN9 mutant, the 5th residue is the first that reaches a probability for formation of an α-helix of ≥50%, whereas in all other cases it is the 2nd or 3rd residue; thus, for a few residues at the extreme N terminus of γΔN9, the helix might be unwound. For γΔN4, the predicted probability for formation of an α-helix by the initial residues is lower than in the other cases but still ≥50% (as compared with 90–100% for the other truncation mutants).

C-truncation mutants of γ: an overview

The C-terminal γ truncation mutants generated for this study were as follows: γΔC14, eliminating 14 residues from the C terminus; γΔC20; γΔC27; γΔC36; and γΔC60. In the γΔC60 mutant, the C terminus is outside of the $\alpha_3\beta_3$ cylinder. According to the crystal structures of the mitochondrial and *E. coli* enzymes (31–33), the C-terminal helix starts 73 and 76 residues, respectively, upstream of the C terminus and runs uninterrupted to the C terminus. Secondary structure predictions (Fig. 1*B*) suggest similar behavior for the C-terminal helix of the *G. stearothermophilus* enzyme, although for the terminal 6–7 residues the probability to form a helix is only about 50%. According to the predictions, also in the truncation mutants the helix reaches close to the respective C terminus.

Stability and ATPase activity of the $\alpha_3\beta_3\gamma$ subcomplexes

An $\alpha_3\beta_3\gamma$ subcomplex could be isolated from each of the five N-terminal truncation mutants and from four of five C-terminal truncation mutants. Of the N-terminal truncation mutants, based on Western blotting using an antibody against the globular portion of γ, the γΔN4 and γΔN9 mutants contained a full complement of γ. In the mutants with longer N-terminal truncations, the amount of γ was substoichiometric. Obviously, these truncations reduce the stability of the interactions of γ with the $\alpha_3\beta_3$ cylinder. Still, even for the γΔN45 mutant in

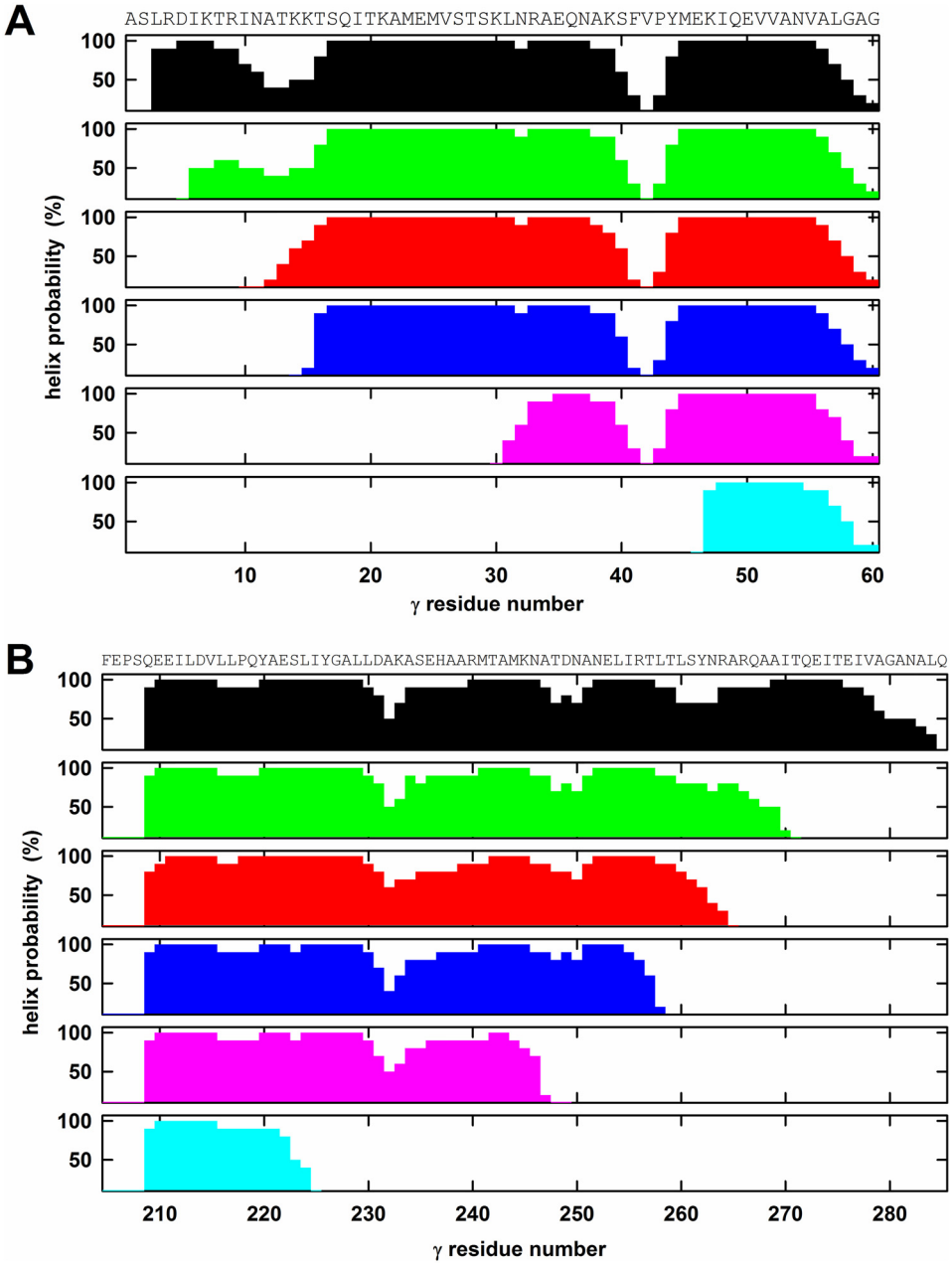

Figure 1. Secondary structure predictions for the γ truncation mutants. All secondary structure predictions were obtained using the PredictProtein server (49). The amino acid sequence is given on *top* of the figure. The figure plots the probability of formation of an α-helix. The *top panels* (*panels 1*; *black*) show the prediction for the WT *G. stearothermophilus* enzyme with full-length γ. It should be noted that the prediction for γ of mitochondrial ATP synthase gave very similar results (not shown) with a lower probability of α-helix formation between residues γ10 and γ15 and a disruption of the helix between γ40 and γ45. The crystal structures (31, 32) show the γ10–15 segment as helical and confirm the helix break around γ40–45. *A*, N-terminal truncations. *Panels 2–6* show the predictions for the N-terminal truncation mutants γΔN4 (*green*), γΔN9 (*red*), γΔN13 (*blue*), γΔN29 (*pink*), and γΔN45 (*cyan*). *B*, C-terminal truncations. *Panels 2–6* show the predictions for the C-terminal mutations γΔC14 (*green*), γΔC20 (*red*), γΔC27 (*blue*), γΔC36 (*pink*), and γΔC60 (*cyan*).

nearly a half of the enzyme complexes γ was still present (Table 1 and Fig. S2*A*). As to the C-terminal mutants, for the longest truncation, γΔC60, an $\alpha_3\beta_3\gamma$ subcomplex could not be isolated. No γ was found in the preparation; instead, an $\alpha_3\beta_3$ subcomplex was obtained (data not shown). Thus, this mutant was not pursued any further. All shorter C-terminal truncations contained stoichiometric amounts of γ (Table 1 and Fig. S2*B*).

Of the $\alpha_3\beta_3\gamma$ subcomplexes with N-terminal truncations, only γΔN4 showed an ATPase activity that was similar to that of the WT enzyme. In the case of the γΔN9 and γΔN13 $\alpha_3\beta_3\gamma$ subcomplexes, the ATPase activity was about 10% of the WT value. For γΔN29 and γΔN45 $\alpha_3\beta_3\gamma$ it was even less but still clearly higher than for a γ-less $\alpha_3\beta_3$ subcomplex (Table 1). Of the C-terminal truncation mutants, again only the shortest one, γΔC14, had an ATPase activity in the same range of that of enzyme with full-length γ. The activity of γΔC20 was about 10% of WT; those of γΔC27 and γΔC36 were 2–3%. Again, even the C-terminal deletion mutants with the largest functional impairment still had ATPase activities significantly higher than the γ-less enzyme (Table 1). A general decrease of the ATPase activity with

Table 1

ATPase activities and ATP-binding properties of γ truncation mutants

The content of γ in the subcomplex preparations was measured by Western blotting using an antibody against the globular portion of γ. Each Western blot contained an $\alpha_3\beta_3\gamma$ control, set as 100%, and an $\alpha_3\beta_3$ control, set as 0%. ATPase activities were determined in duplicate at 42 °C and pH 8.0 by the amount of P_i released. Nucleotide binding to the three catalytic sites was measured at 23 °C and pH 8.0 using the fluorescence of residue βTrp[341] as signal. This technique does not allow resolving K_d values below 0.01 μM with confidence. All values given in this table represent the average from at least two independent experiments with two different enzyme preparations with standard deviations in parentheses.

Enzyme/ mutation	Content of γ	ATPase activity	MgATP binding		
			K_{d1}	K_{d2}	K_{d3}
	%	*units/mg*	μM		
$\alpha_3\beta_3\gamma$	100	17 (3)	<0.010	4.4 (0.7)	29 (6)
$\alpha_3\beta_3$	0	0.09 (0.08)	2.2 (0.7)	10 (2)	11 (2)
γΔN4	99 (5)	25 (5)	<0.010	1.9 (0.6)	54 (22)
γΔN9	103 (6)	2.2 (0.2)	0.41 (0.12)	13 (2)	13 (2)
γΔN13	67 (10)	1.7 (0.4)	2.2 (0.8)	13 (2)	13 (2)
γΔN29	53 (8)	0.30 (0.03)	1.4 (0.5)	15 (3)	16 (3)
γΔN45	46 (9)	0.55 (0.12)	1.2 (0.2)	11 (2)	11 (2)
γΔC14	95 (8)	11 (2)	0.015 (0.003)	4.0 (1.0)	23 (7)
γΔC20	104 (12)	1.4 (0.3)	0.012 (0.003)	3.0 (0.8)	16 (5)
γΔC27	114 (20)	0.48 (0.13)	1.1 (0.3)	11 (2)	11 (2)
γΔC36	110 (22)	0.43 (0.13)	1.8 (0.3)	13 (2)	13 (2)
γA^{5-10}	ND[a]	13 (2)	<0.010	3.7 (0.9)	16 (4)
γA^{10-15}	ND	18 (2)	<0.010	4.8 (1.3)	15 (5)
$\gamma A^{256-260}$	ND	31 (6)	<0.010	3.4 (0.7)	25 (6)
$\gamma A^{260-265}$	ND	30 (6)	<0.010	2.8 (0.8)	17 (6)

[a] ND, not determined; as all alanine replacement mutants showed wildtype-like activities and MgATP binding pattern, measurement of the γ content seemed unnecessary.

the length of the deletion had been described before for N-terminal as well as C-terminal truncations (23, 25, 26).

Effect of truncations on MgATP binding

The fluorescence of residue βTrp[341] in the $\alpha_3\beta_3\gamma$ subcomplex was used to determine the MgATP binding properties of the truncation mutants. The results are compiled in Fig. 2, *A* (N-terminal truncations) and *B* (C-terminal truncations), and in Table 1. MgATP binding data for the WT $\alpha_3\beta_3\gamma$ subcomplex and the γ-less subcomplex, $\alpha_3\beta_3$, are shown as controls. $\alpha_3\beta_3\gamma$ shows the well-established MgATP binding asymmetry with a K_{d1} below 10 nM, a K_{d2} of about 4 μM, and a K_{d3} of about 30 μM. For the $\alpha_3\beta_3$ subcomplex, in the absence of γ, it had been shown previously that it has a highly symmetrical structure (29) and has lost its ability to bind MgTNP-ATP[5] and MgTNP-ADP with high affinity (34). Here, we confirmed the "functional symmetry" of the $\alpha_3\beta_3$ subcomplex. High-affinity binding was not observed, and the three catalytic binding sites had very similar affinities for MgATP. An optimal fit was obtained using a model with three different sites; the fit suggested that one of the three sites might still have a slightly higher affinity than the remaining two sites. However, as can be seen from Fig. 2 (best visible in *C*), the difference between this fit (*solid black line* through the *open circles*) and the fit for a model with three identical sites (*dotted black line*) is minimal. In the latter case, $K_{d123} = 6.1$ μM.

In the nucleotide binding experiments, both series of truncation mutants showed the same tendencies, from a WT-like asymmetrical pattern with a clearly expressed high-affinity binding site for the shorter truncations to a symmetrical binding behavior with a loss of the high-affinity site for the longer

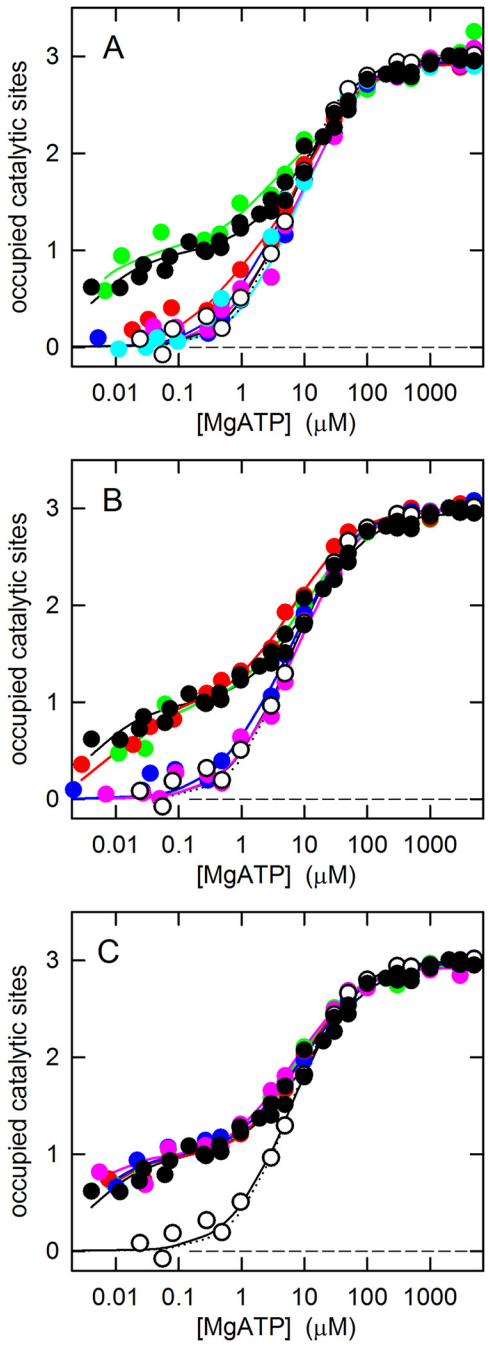

Figure 2. MgATP binding to the catalytic sites of the γ truncation and alanine-replacement mutants. MgATP binding to the three catalytic sites of the $\alpha_3\beta_3\gamma$ subcomplex of *G. stearothermophilus* ATP synthase was measured as described under "Experimental procedures." In all panels, WT $\alpha_3\beta_3\gamma$ with full-length γ is represented by *black filled circles*, and $\alpha_3\beta_3$ (no γ) is represented by *white open circles*. Each plot shows a representative experiment, combining data from four independent titrations, with the MgATP concentration increased by an order of magnitude in each step (8). The *solid lines* are fitted binding curves based on a model with three different, independent sites. K_d values are given in Table 1. For the γ-less $\alpha_3\beta_3$ subcomplex, the fit based on a model with identical sites is also shown (*dotted black lines*). *A*, N-terminal truncation mutants: γΔN4, *green*; γΔN9, *red*; γΔN13, *blue*; γΔN29, *pink*; γΔN45, *cyan*. *B*, C-terminal truncation mutants γΔC14, *green*; γΔC20, *red*; γΔC27, *blue*; γΔC36, *pink*. *C*, alanine-replacement mutants: γA^{5-10}, *green*; γA^{10-15}, *red*; $\gamma A^{256-260}$, *blue*; $\gamma A^{260-265}$, *pink*.

truncations. Of the N-terminal truncation mutants, only γΔN4 displayed strong asymmetric behavior (Fig. 2*A*); of the C-terminal truncations, both γΔC14 and γΔC20 did (Fig. 2*B*). In con-

[5] The abbreviations used are: TNP, trinitrophenyl; CDTA, *trans*-1,2-diaminocyclohexane-*N*,*N*,*N*′,*N*′-tetraacetic acid.

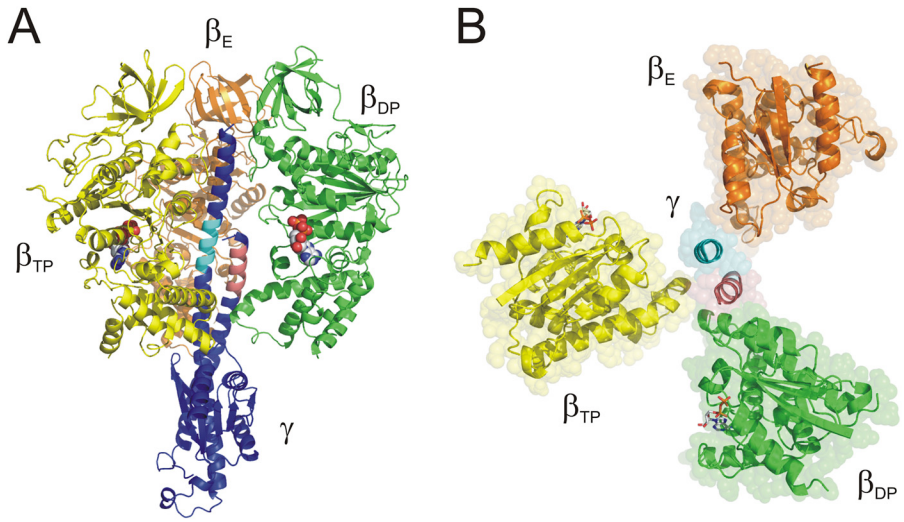

Figure 3. Identification of the segments in the N- and C-terminal helices of γ responsible for the affinity differences of the catalytic sites. *A*, side view. The identified segment in the N-terminal helix, γ5–15, is shown in *pink*; the segment in the C-terminal helix, γ256–265, is shown in *cyan*; and the remainder of γ is shown in *purple*. Subunit β_{TP}, which carries the high-affinity nucleotide-binding site, is shown in *yellow*; subunit β_{DP} with the medium-affinity binding site is colored *green*, and subunit β_E is *orange*. Bound nucleotides are shown as "*space-filled*"; the site on β_E is empty in the crystal structure. For clarity, the α subunits have been removed. *B*, top view, looking toward the membrane. Color-coding is as in *A*. Bound nucleotides are shown in "*stick*" representation. The portion of the β subunits above the level of the nucleotide-binding sites has been removed. γ is represented just by the two segments, γ5–15 and γ256–265. Segment γ5–15 makes contact with the DELSEED loop of subunits β_{TP} and β_{DP}; segment γ256–265 makes contact with the catch loop of subunit β_E (for further details, see "Results" and "Discussion").

trast, $\gamma\Delta$N13, $\gamma\Delta$N29, and $\gamma\Delta$N45 exhibited the (nearly) symmetrical binding pattern of the γ-less enzyme as did $\gamma\Delta$C27 and $\gamma\Delta$C36. Whereas for the C-terminal truncations the binding pattern went directly from WT-like in $\gamma\Delta$C20 to γ-less-like in $\gamma\Delta$C27, among the N-terminal truncations $\gamma\Delta$N9 presented a transition case. The affinity of site 1 in $\gamma\Delta$N9 appeared to be slightly higher than in the mutants with longer truncations.

As noted above, in $\gamma\Delta$N13, $\gamma\Delta$N29, and $\gamma\Delta$N45, the amount of γ was substoichiometric. Nevertheless, as these mutants display binding characteristics that are virtually indistinguishable from those of $\alpha_3\beta_3$, correction of the binding curves for "contamination" by γ-less enzyme did not change the results significantly. However, this correction assumes that the amount of γ in the $\alpha_3\beta_3\gamma$ subcomplex remains constant during the binding assay. To test whether this assumption is valid, we concentrated the assay mixture after the binding assay using a Centricon centrifugal filter device with an exclusion limit of 50,000 Da, which would let isolated γ pass through. Immunoblot analysis of the concentrate indicated that for $\gamma\Delta$N29 and $\gamma\Delta$N45 the amount of γ in the $\alpha_3\beta_3\gamma$ subcomplex was indeed further reduced by 30–50%. However, the $\gamma\Delta$N13 $\alpha_3\beta_3\gamma$ subcomplex showed the same amount of γ as before the binding experiment (Fig. S2*C*). Thus, there is no doubt that $\gamma\Delta$N13 displays a symmetrical binding pattern, just as γ-less enzyme. Although the precise amount of γ in the $\alpha_3\beta_3\gamma$ subcomplex of $\gamma\Delta$N29 and $\gamma\Delta$N45 at the exact moment of the binding assay is not known and therefore a correction for the contamination by γ-less enzyme is not straightforward, it appears highly unlikely that these truncation mutants would revert to an asymmetric pattern.

The segments of γ responsible for the nucleotide binding asymmetry of the catalytic sites: N terminus

At the N terminus, truncation of just 4 residues preserved the asymmetric WT binding pattern. Truncation of 13 or more residues resulted in the symmetric pattern seen in the absence of γ. Truncation of 9 residues showed intermediate characteristics with a higher degree of asymmetry than observed for the longer truncations but no pronounced high-affinity binding site. Based on the results, one might conclude that the segment most important for determination of the affinities of the three catalytic sites consists of residues γ5–9. However, it is possible that the failure of the $\gamma\Delta$N9 truncation mutant to give a WT-like binding pattern (like $\gamma\Delta$N4) could be due to failure to form an α-helix immediately at its N terminus (see "Results" and Fig. 1). In contrast to $\gamma\Delta$N9, secondary predictions for $\gamma\Delta$N13 indicate that this mutant reaches α-helical conformation within 2–3 residues. Thus, the affinity-determining segment on the N-terminal helix should not extend beyond residue γ15, giving it the sequence γ^5DIKTRINATKK^{15}.

None of the residues of the γ^5DIKTRINATKK^{15} segment is completely conserved; however, several display exclusively conservative substitutions (Table S1). In general, positions γ7–γ15 show an accumulation of arginine and lysine residues, between 2 and 5 in the examples shown; the net charge of this stretch is between +1 and +5. The γ5–15 segment comes close to three subunits of the $\alpha_3\beta_3$ cylinder, β_{TP},[6] β_{DP}, and α_E (Figs. 3*A* and S3*A*). In the structure of the *E. coli* enzyme (33), γ5–15 also has contacts with the C-terminal helix of the ϵ subunit. Possible interactions with β_{TP} and β_{DP} occur with the DELSEED loop of these subunits. The multiple negatively charged side chains of the DELSEED loop appear well suited for interactions with the positive charges of the γ5–15

[6] The nomenclature of α and β subunits is based on the nucleotide occupancy of the catalytic sites in the original structure of the mitochondrial enzyme (31). Subunits α_{TP} and β_{TP} contribute to formation of the catalytic site occupied by a non-hydrolyzable ATP analog, AMP-PNP (5′-adenylyl-β,γ-imidodiphosphate); α_{DP} and β_{DP} contribute to formation of the catalytic site occupied by ADP; and α_E and β_E contribute to formation of the empty catalytic site.

segment. However, it has been shown that the negative charges of the DELSEED motif can be removed without affecting enzymatic activity, MgATP binding asymmetry, and rotational torque (35–38).

The segments of γ responsible for the nucleotide binding asymmetry of the catalytic sites: C terminus

At the C terminus, truncation of up to 20 residues gave the asymmetric, WT-like binding pattern, whereas removal of 27 or more residues resulted in the symmetric pattern, lacking a high-affinity binding site, also observed in the absence of γ. Thus, the affinity-determining segment of the C-terminal helix should, at the minimum, consist of residues γ^{259}TLSYNRA^{265}, which are present in γΔC20 but absent in γΔC27. Taking into account that the terminal residues of γΔC27 might not be in quite the same helical confirmation as in full-length γ, a reasonable estimate for the C-terminal affinity-determining segment appears to be γ^{256}RTLTLSYNRA^{265}. Of these residues, γAsn^{263} is conserved; several other positions contain exclusively conservative substitutions (Table S2).

Is it possible to identify the residue(s) responsible for the nucleotide binding asymmetry?

To answer this question, all residues in the two identified segments were replaced by alanine. We made two alanine mutants per segment by replacing 5–6 residues at a time by alanine because making longer alanine mutants was challenging. Thus, we generated the mutations γA$^{5-10}$, γA$^{10-15}$, γA$^{256-260}$, and γA$^{260-265}$ for N- and C-terminal segments, respectively.

The results of the functional assays are shown in Table 1 and Fig. 2*C*. All four mutant enzymes had WT-like ATPase activity and a WT-like asymmetric MgATP binding pattern. Thus, it seems that no specific interaction between amino acid side chains in γ and β (or α) causes the binding asymmetry. Instead, it appears as if the α-helices themselves in this region are responsible.

Discussion

One major goal of the research on ATP synthase in our lab at this time is to explore the molecular basis for the changes in affinity of the catalytic sites during rotation and to analyze the role of these affinity changes in coupling of catalysis and rotation. The affinity of a catalytic site for substrate(s) and product(s) at any given point of time is determined by the position of the central γ subunit. In the absence of γ, all three sites have the same, rather low affinity. Several residues at the β/γ interface that affect binding affinities of the catalytic sites have been described before (14, 15, 39). In the present study, we aimed to identify the part(s) of γ that included all residues that are responsible for the affinity differences. For this purpose, we measured nucleotide binding to the catalytic sites of two series of γ truncation mutants, one that had between 4 and 45 residues from the N terminus of γ removed and the other between 14 and 60 residues from the C terminus. The truncations were done using the enzyme from *G. stearothermophilus* because of its superior oligomeric stability. In the absence of γ, it can form a stable $\alpha_3\beta_3$ complex (28), which has not yet been described for the *E. coli* enzyme. However, both enzymes are functionally so similar, specifically in their nucleotide binding pattern (for comparison, see the K_d(MgATP) values for *E. coli* given in the Introduction and the *G. stearothermophilus* values in Table 1), that there is no reason to assume that these patterns were achieved by different mechanisms.

The truncation approach yielded two segments of about 10 residues, one on the N-terminal helix, γ5–15, and the other on the C-terminal helix, γ256–265. Both segments are required to give the asymmetric, WT-like nucleotide binding pattern with pronounced affinity differences and a clearly expressed high-affinity site. If one of them is missing, the enzyme shows the symmetric binding behavior with a relatively low overall affinity that is also observed in the complete absence of γ.

Over both segments, about half of the residues are conserved or conservatively substituted (see "Results" and Tables S1 and S2), and a number of these residues are able to form hydrogen bonds and/or salt bridges with residues on the α or β subunits (Fig. S3). However, experiments where the residues in both segments were replaced by alanine gave a WT-like asymmetric nucleotide binding pattern and WT-like catalytic activity. Thus, no individual amino acid side chains appear to be responsible for asymmetry and activity. This finding is reminiscent of the βDELSEED loop, which is essential for driving γ rotation and enzymatic activity due to its overall bulk shape, without individual interactions between amino acid side chains required for its function (35–38).

The affinity-determining segment of the N-terminal helix, γ5–15, makes contact with the DELSEED loop of the β_{TP} and β_{DP} subunits, which carry the high- and medium-affinity catalytic site, respectively (18). This observation confirms the importance of the DELSEED loop in affinity regulation of the catalytic sites as suggested by previous studies (14, 15). Absence of the γ5–15 segment apparently fails to bring the respective β subunit into the high- or medium-affinity conformation. The affinity-determining segment of the C-terminal helix, γ256–265, is located at a level similar to its N-terminal counterpart, γ5–15, offset by approximately one helical turn in direction away from the membrane (Fig. 3). A portion of the γ256–265 segment approaches the "catch loop" (31, 40) of the β_E subunit, residues β309–316. The γΔC27 truncation removes any interaction of the C-terminal helix with the catch loop. Considering that the affinity of the low-affinity catalytic site on β_E is not affected by γ, it seems possible that the role of this segment in determination of the affinity of the catalytic sites on β_{TP} and β_{DP} is indirect, by stabilizing the N-terminal γ5–15 segment and its interactions with $\alpha_3\beta_3$. Theoretically, it would also be possible that lack of this portion of the C-terminal helix might cause failure to form the N-terminal helix (41). However, we could show that a γ subunit consisting just of the N-terminal 35 or 42 residues was able to sustain a certain degree of ATP synthesis activity (19), which would be highly unlikely if the segment were unstructured. Furthermore, it has been shown that truncation of the N terminus by 50 residues (26) or of the C terminus by 36 residues (25) still allows production of torque close to 50% of WT, whereas the torque generated by an enzyme without both helices is significantly lower (24). Taken together, these findings suggest that each of the helices can

exist without support of the other. Thus, the structural integrity of γ is preserved in the truncation mutants.

Interestingly, despite the presence of a high-affinity site, the γΔC20 truncation mutant showed only low ATPase activity; adding back 6 more residues, in the γΔC14 mutant, restored WT-like activities. This finding is in contrast to the situation at the N terminus where the presence of a high-affinity site went hand in hand with normal ATPase activities as observed with γΔN4; the γΔN9 mutant, which had largely lost high-affinity binding capability, also had substantially reduced enzymatic activity. Thus, as far as the mutants under investigation here are concerned, the presence of a high-affinity site appears to be a necessary, but not sufficient, condition for high activity.

The 2 residues immediately downstream of the identified segment, γArg^{266} and γGln^{267} are strictly conserved. However, from the results presented here, it is clear that they have no influence on the binding affinity of the catalytic sites as these residues are missing in γΔC20, which nevertheless has a WT-like binding pattern. Given the importance of γArg^{266} and γGln^{267} for the catalytic function (40, 42),[7] it is likely that their absence in γΔC20 is responsible for the low enzymatic activity of this truncation mutant. The lack of residue γThr^{271} in γΔC20 (which is present in γΔC14) could be another factor for its catalytic impairment (42, 43). It is interesting to note that loss of hydrogen-bonding capability of γThr^{271} resulted in reduced nucleotide-binding affinity of the catalytic site(s) in the transition state (measured as rate of formation of the transition-state analog MgADP–fluoroaluminate complex (43)). However, as the results presented here show, γThr^{271} has no role in determining the affinity in the ground state.

Experimental procedures

Bacterial strains and plasmids

For generation of the γ truncation mutants in *G. stearothermophilus* $\alpha_3\beta_3\gamma$ and the γ-less $\alpha_3\beta_3$ subcomplexes, the background plasmid was pNM2. Plasmid pNM2 is a derivative of plasmid pKAGB1 (44). pKAGB1 is used to express a Cys- and Trp-less form of the $\alpha_3\beta_3\gamma$ subcomplex of *G. stearothermophilus* ATP synthase. pNM2 contains an additional mutation to generate an $\alpha_3(\beta Y341W)_3\gamma$ subcomplex, which allows monitoring nucleotide binding to the three catalytic sites, and a His_{10} tag at the N terminus of the β subunits to facilitate purification. Site-directed mutagenesis was performed using the QuikChange II XL kit. To generate the N-terminal truncations, downstream of the γ start codon ATG, the codons for the next 4–45 amino acids were eliminated. To obtain the C-terminal truncations, stop codons were inserted at the desired positions. For generation of the γ-less enzyme, a stop codon was introduced at the γ7 position. The insertion of an NheI site downstream of this stop codon allowed us to remove the remainder of the gene for γ on an NheI-NheI fragment as there is a natural NheI site downstream of the γ gene. Removal of segments was confirmed by DNA sequencing of the plasmid product. For expression of the mutant proteins, the plasmids were transformed into *E. coli* strain JM103Δ(*uncB-uncD*).

Isolation of $\alpha_3\beta_3(\gamma)$ subcomplex and quantification of truncated γ subunit

The purification method of $\alpha_3\beta_3\gamma$ or $\alpha_3\beta_3$ subcomplex was modified from a previously described procedure (45). Cells were grown aerobically at 37 °C in terrific broth medium containing 100 μg/ml ampicillin. After cell lysis by French press, the cell debris was removed by centrifugation at 35,000 rpm for 30 min. The supernatant containing the complex was applied to a Ni^{2+}-nitrilotriacetic acid column (Qiagen) equilibrated with 20 mM imidazole and 100 mM NaCl, pH 7.0. The column was washed with 50 mM imidazole and 100 mM NaCl, pH 7.0, and the enzyme was eluted with 500 mM imidazole and 100 mM NaCl, pH 7.0. The subcomplex was stored as precipitate in 70% saturated ammonium sulfate at 4 °C. The amount of truncated γ subunit was determined via Western blotting using antibodies raised against a peptide corresponding to a part of the globular portion of γ; the antibodies were a kind gift from Drs. Toshiharu Suzuki and Masasuke Yoshida (Japan Science and Technology Agency, Tokyo, Japan). $\alpha_3\beta_3\gamma$ subcomplex with full-length γ served as a standard. Blots were then developed with enhanced chemoluminescence substrate (Thermo Scientific). The expression level of γ subunit was quantified by measuring the integrated density of bands using a Photodyne imaging system and NIH ImageJ acquisition software. Control experiments with an anti-β antibody (Agrisera, Vännäs, Sweden) showed that the amount of β was not affected by the mutations (Fig. S2, *A* and *B*).

The oligomeric state of $\alpha_3\beta_3\gamma$ and $\alpha_3\beta_3$ samples was assessed by size exclusion chromatography. A Bio-Sil SEC 250 7.8 × 80-mm column, equilibrated with 100 mM sodium phosphate buffer, pH 6.8, was used. The eluate was monitored by UV absorbance at 280 nm. The calculated molecular masses of $\alpha_3\beta_3\gamma$ and $\alpha_3\beta_3$ complexes and α and β individual subunits, based on their amino acid sequences, are 352, 320, 55, and 52 kDa, respectively. BSA (66 kDa) and bovine heart lactate dehydrogenase (137 kDa) were used as controls.

Functional analysis of mutant enzymes

ATPase activities were assayed in a buffer containing 50 mM Tris/H_2SO_4, 10 mM ATP, and 4 mM $MgSO_4$, pH 8.0, at 42 °C. The reaction was started by addition of 10–20 μg/ml enzyme and stopped after 1 or 2 min (depending on the activity) by addition of SDS (final concentration, 5%, w/v). The released P_i was measured as described (46). 1 unit of enzymatic activity corresponds to 1 μmol of ATP hydrolyzed (equivalent to 1 μmol of P_i produced)/min.

Binding of MgATP to the catalytic sites of the purified $\alpha_3\beta_3$ or $\alpha_3\beta_3\gamma$ subcomplex was measured using the fluorescence of the inserted Trp residue βTrp^{341} (7, 8). Before use, the $\alpha_3\beta_3\gamma$ ammonium sulfate precipitate was pelleted by centrifugation and redissolved in a buffer containing 50 mM Tris/HCl and 10 mM CDTA, pH 8.0. After 1-h incubation at 23 °C, the $\alpha_3\beta_3\gamma$ subcomplex was passed through two subsequent centrifuge columns containing Sephadex G-50 equilibrated with 50 mM Tris/HCl and 0.1 mM EDTA, pH 8.0. After this treatment, the

[7] The cited references use the *E. coli* enzyme. Although at the N terminus of γ the amino acid numbers for *G. stearothermophilus* and *E. coli* are the same, at the C terminus adding 2 to the *G. stearothermophilus* numbers gives those for *E. coli*.

enzyme subcomplex is essentially nucleotide-free (47); using the luciferin/luciferase method after heat denaturation of the enzyme complex, we found <0.1 mol of nucleotide (ATP plus ADP)/mol of subcomplex. To measure MgATP binding, fluorescence titrations were performed in a buffer containing 50 mM Tris/H_2SO_4 and 2.5 mM $MgSO_4$, pH 8.0, with ATP added to the desired concentration. K_d values were determined by fitting of theoretical curves to the experimental data points by nonlinear least-squares analysis. All functional assays were performed within 2–3 days after preparation of the enzyme.

Miscellaneous

Protein concentrations were determined by the method of Bradford (48) using BSA as a standard. Secondary structure predictions were performed using the PredictProtein server (49). Figs. 3 and S3 were created using PyMOL (Schrödinger, Portland, OR) using Protein Data Bank code 1E79 (32) as starting material.

Author contributions—N. M. and Y. L. data curation; N. M., Y. L., and J. W. formal analysis; N. M. and Y. L. investigation; N. M., Y. L., and J. W. writing-review and editing; J. W. conceptualization; J. W. supervision; J. W. funding acquisition; J. W. writing-original draft; J. W. project administration.

Acknowledgment—We thank Cristina Pinal for valuable technical assistance.

References

1. Weber, J., and Senior, A. E. (2003) ATP synthesis driven by proton transport in F_1F_o-ATP synthase. *FEBS Lett.* **545,** 61–70 CrossRef Medline
2. Nakamoto, R. K., Baylis Scanlon, J. A., and Al-Shawi, M. K. (2008) The rotary mechanism of the ATP synthase. *Arch. Biochem. Biophys.* **476,** 43–50 CrossRef Medline
3. von Ballmoos, C., Wiedenmann, A., and Dimroth, P. (2009) Essentials for ATP synthesis by F_1F_0 ATP synthases. *Annu. Rev. Biochem.* **78,** 649–672 CrossRef Medline
4. Watanabe, R., and Noji, H. (2013) Chemomechanical coupling mechanism of F_1-ATPase: catalysis and torque generation. *FEBS Lett.* **587,** 1030–1035 CrossRef Medline
5. Junge, W., and Nelson, N. (2015) ATP synthase. *Annu. Rev. Biochem.* **84,** 631–657 CrossRef Medline
6. Nakanishi-Matsui, M., Sekiya, M., and Futai, M. (2016) ATP synthase from *Escherichia coli*: mechanism of rotational catalysis, and inhibition with the ϵ subunit and phytopolyphenols. *Biochim. Biophys. Acta* **1857,** 129–140 CrossRef Medline
7. Weber, J., Wilke-Mounts, S., Lee, R. S., Grell, E., and Senior, A. E. (1993) Specific placement of tryptophan in the catalytic sites of *Escherichia coli* F_1-ATPase provides a direct probe of nucleotide binding: maximal ATP hydrolysis occurs with three sites occupied. *J. Biol. Chem.* **268,** 20126–20133 Medline
8. Weber, J., and Senior, A. E. (2004) Fluorescent probes applied to catalytic cooperativity in ATP synthase. *Methods Enzymol.* **380,** 132–152 CrossRef Medline
9. Nishizaka, T., Oiwa, K., Noji, H., Kimura, S., Muneyuki, E., Yoshida, M., and Kinosita, K., Jr. (2004) Chemomechanical coupling in F_1-ATPase revealed by simultaneous observation of nucleotide kinetics and rotation. *Nat. Struct. Mol. Biol.* **11,** 142–148 CrossRef Medline
10. Adachi, K., Oiwa, K., Nishizaka, T., Furuike, S., Noji, H., Itoh, H., Yoshida, M., and Kinosita, K., Jr. (2007) Coupling of rotation and catalysis in F_1-ATPase revealed by single-molecule imaging and manipulation. *Cell* **130,** 309–321 CrossRef Medline
11. Watanabe, R., Iino, R., and Noji, H. (2010) Phosphate release in F_1-ATPase catalytic cycle follows ADP release. *Nat. Chem. Biol.* **6,** 814–820 CrossRef Medline
12. Watanabe, R., and Noji, H. (2014) Timing of inorganic phosphate release modulates the catalytic activity of ATP-driven rotary motor protein. *Nat. Commun.* **5,** 3486 CrossRef Medline
13. Weber, J. (2010) Structural biology: Toward the ATP synthase mechanism. *Nat. Chem. Biol.* **6,** 794–795 CrossRef Medline
14. Scanlon, J. A., Al-Shawi, M. K., and Nakamoto, R. K. (2008) A rotor-stator cross-link in the F_1-ATPase blocks the rate-limiting step of rotational catalysis. *J. Biol. Chem.* **283,** 26228–26240 CrossRef Medline
15. Mnatsakanyan, N., Krishnakumar, A. M., Suzuki, T., and Weber, J. (2009) The role of the βDELSEED-loop of ATP synthase. *J. Biol. Chem.* **284,** 11336–11345 CrossRef Medline
16. Scanlon, J. A., Al-Shawi, M. K., Le, N. P., and Nakamoto, R. K. (2007) Determination of the partial reactions of rotational catalysis in F_1-ATPase. *Biochemistry* **46,** 8785–8797 CrossRef Medline
17. Gao, Y. Q., Yang, W., and Karplus, M. (2005) A structure-based model for the synthesis and hydrolysis of ATP by F_1-ATPase. *Cell* **123,** 195–205 CrossRef Medline
18. Mao, H. Z., and Weber, J. (2007) Identification of the βTP site in the x-ray structure of F_1-ATPase as the high-affinity catalytic site. *Proc. Natl. Acad. Sci. U.S.A.* **104,** 18478–18483 CrossRef Medline
19. Mnatsakanyan, N., Hook, J. A., Quisenberry, L., and Weber, J. (2009) ATP synthase with its γ subunit reduced to the N-terminal helix can still catalyze ATP synthesis. *J. Biol. Chem.* **284,** 26519–26525 CrossRef Medline
20. Pu, J., and Karplus, M. (2008) How subunit coupling produces the γ-subunit rotary motion in F_1-ATPase. *Proc. Natl. Acad. Sci. U.S.A.* **105,** 1192–1197 CrossRef Medline
21. Yasuda, R., Noji, H., Yoshida, M., Kinosita, K., Jr, and Itoh, H. (2001) Resolution of distinct rotational substeps by submillisecond kinetic analysis of F_1-ATPase. *Nature* **410,** 898–904 CrossRef Medline
22. Shimabukuro, K., Yasuda, R., Muneyuki, E., Hara, K. Y., Kinosita, K., Jr, and Yoshida, M. (2003) Catalysis and rotation of F_1 motor: cleavage of ATP at the catalytic site occurs in 1 ms before 40° substep rotation. *Proc. Natl. Acad. Sci. U.S.A.* **100,** 14731–14736 CrossRef Medline
23. Hossain, M. D., Furuike, S., Maki, Y., Adachi, K., Ali, M. Y., Huq, M., Itoh, H., Yoshida, M., and Kinosita, K., Jr. (2006) The rotor tip inside a bearing of a thermophilic F_1-ATPase is dispensable for torque generation. *Biophys. J.* **90,** 4195–4203 CrossRef Medline
24. Furuike, S., Hossain, M. D., Maki, Y., Adachi, K., Suzuki, T., Kohori, A., Itoh, H., Yoshida, M., and Kinosita, K., Jr. (2008) Axle-less F_1-ATPase rotates in the correct direction. *Science* **319,** 955–958 CrossRef Medline
25. Hossain, M. D., Furuike, S., Maki, Y., Adachi, K., Suzuki, T., Kohori, A., Itoh, H., Yoshida, M., and Kinosita, K., Jr. (2008) Neither helix in the coiled coil region of the axle of F_1-ATPase plays a significant role in torque production. *Biophys. J.* **95,** 4837–4844 CrossRef Medline
26. Kohori, A., Chiwata, R., Hossain, M. D., Furuike, S., Shiroguchi, K., Adachi, K., Yoshida, M., and Kinosita, K., Jr. (2011) Torque generation in F_1-ATPase devoid of the entire amino-terminal helix of the rotor that fills half of the stator orifice. *Biophys J* **101,** 188–195 CrossRef Medline
27. Steffens, K., Di Gioia, A., Deckers-Hebestreit, G., and Altendorf, K. (1987) Structural and functional relationship of ATP synthases (F_1F_o) from *Escherichia coli* and the thermophilic bacterium PS3. *J. Biol. Chem.* **262,** 6334–6338 Medline
28. Miwa, K., and Yoshida, M. (1989) The $\alpha_3\beta_3$ complex, the catalytic core of F_1-ATPase. *Proc. Natl. Acad. Sci. U.S.A.* **86,** 6484–6487 CrossRef Medline
29. Shirakihara, Y., Leslie, A. G., Abrahams, J. P., Walker, J. E., Ueda, T., Sekimoto, Y., Kambara, M., Saika, K., Kagawa, Y., and Yoshida, M. (1997) The crystal structure of the nucleotide-free $\alpha_3\beta_3$ subcomplex of F_1-ATPase from the thermophilic *Bacillus* PS3 is a symmetric trimer. *Structure* **5,** 825–836 CrossRef Medline
30. Uchihashi, T., Iino, R., Ando, T., and Noji, H. (2011) High-speed atomic force microscopy reveals rotary catalysis of rotorless F_1-ATPase. *Science* **333,** 755–758 CrossRef Medline
31. Abrahams, J. P., Leslie, A. G., Lutter, R., and Walker, J. E. (1994) Structure at 2.8 Å resolution of F_1-ATPase from bovine heart mitochondria. *Nature* **370,** 621–628 CrossRef Medline

32. Gibbons, C., Montgomery, M. G., Leslie, A. G., and Walker, J. E. (2000) The structure of the central stalk in bovine F_1-ATPase at 2.4 Å resolution. *Nat. Struct. Biol.* **7,** 1055–1061 CrossRef Medline
33. Cingolani, G., and Duncan, T. M. (2011) Structure of the ATP synthase catalytic complex (F_1) from *Escherichia coli* in an autoinhibited conformation. *Nat Struct Mol Biol* **18,** 701–707 CrossRef Medline
34. Kaibara, C., Matsui, T., Hisabori, T., and Yoshida, M. (1996) Structural asymmetry of F_1-ATPase caused by the γ subunit generates a high affinity nucleotide binding site. *J. Biol. Chem.* **271,** 2433–2438 CrossRef Medline
35. Hara, K. Y., Noji, H., Bald, D., Yasuda, R., Kinosita, K., Jr, and Yoshida, M. (2000) The role of the DELSEED motif of the β subunit in rotation of F_1-ATPase. *J. Biol. Chem.* **275,** 14260–14263 CrossRef Medline
36. Mnatsakanyan, N., Kemboi, S. K., Salas, J., and Weber, J. (2011) The β subunit loop that couples catalysis and rotation in ATP synthase has a critical length. *J. Biol. Chem.* **286,** 29788–29796 CrossRef Medline
37. Tanigawara, M., Tabata, K. V., Ito, Y., Ito, J., Watanabe, R., Ueno, H., Ikeguchi, M., and Noji, H. (2012) Role of the DELSEED loop in torque transmission of F_1-ATPase. *Biophys. J.* **103,** 970–978 CrossRef Medline
38. Watanabe, R., Koyasu, K., You, H., Tanigawara, M., and Noji, H. (2015) Torque transmission mechanism via DELSEED loop of F_1-ATPase. *Biophys. J.* **108,** 1144–1152 CrossRef Medline
39. Boltz, K. W., and Frasch, W. D. (2006) Hydrogen bonds between the α and β subunits of the F_1-ATPase allow communication between the catalytic site and the interface of the β catch loop and the γ subunit. *Biochemistry* **45,** 11190–11199 CrossRef Medline
40. Greene, M. D., and Frasch, W. D. (2003) Interactions among γ R268, γ Q269, and the β subunit catch loop of *Escherichia coli* F_1-ATPase are important for catalytic activity. *J. Biol. Chem.* **278,** 51594–51598 CrossRef Medline
41. Lumb, K. J., Carr, C. M., and Kim, P. S. (1994) Subdomain folding of the coiled coil leucine zipper from the bZIP transcriptional activator GCN4. *Biochemistry* **33,** 7361–7367 CrossRef Medline
42. Iwamoto, A., Miki, J., Maeda, M., and Futai, M. (1990) H^+-ATPase γ subunit of *Escherichia coli*. Role of the conserved carboxyl-terminal region. *J. Biol. Chem.* **265,** 5043–5048 Medline
43. Boltz, K. W., and Frasch, W. D. (2005) Interactions of γ T273 and γ E275 with the β subunit PSAV segment that links the γ subunit to the catalytic site Walker homology B aspartate are important to the function of *Escherichia coli* F_1F_o ATP synthase. *Biochemistry* **44,** 9497–9506 CrossRef Medline
44. Matsui, T., and Yoshida, M. (1995) Expression of the wild-type and the Cys-/Trp-less $\alpha_3\beta_3\gamma$ complex of thermophilic F_1-ATPase in *Escherichia coli*. *Biochim. Biophys. Acta* **1231,** 139–146 CrossRef Medline
45. Adachi, K., Noji, H., and Kinosita, K., Jr. (2003) Single-molecule imaging of rotation of F_1-ATPase. *Methods Enzymol.* **361,** 211–227 CrossRef Medline
46. Taussky, H. H., and Shorr, E. (1953) A microcolorimetric method for the determination of inorganic phosphorus. *J. Biol. Chem.* **202,** 675–685 Medline
47. Ren, H., Bandyopadhyay, S., and Allison, W. S. (2006) The α_3(βMet222Ser/Tyr345Trp)$_3\gamma$ subcomplex of the TF_1-ATPase does not hydrolyze ATP at a significant rate until the substrate binds to the catalytic site of the lowest affinity. *Biochemistry* **45,** 6222–6230 CrossRef Medline
48. Bradford, M. M. (1976) A rapid and sensitive method for the quantitation of microgram quantities of protein utilizing the principle of protein-dye binding. *Anal. Biochem.* **72,** 248–254 CrossRef Medline
49. Rost, B., Yachdav, G., and Liu, J. (2004) The PredictProtein server. *Nucleic Acids Res.* **32,** W321–W326 CrossRef Medline